ADVANCED FUNCTIONAL MATERIALS
www.afm-journal.de

Effect of Exchange Interactions on the Coercivity of $SmCo_5$ Nanoparticles Made by Cluster Beam Deposition

*O. Akdogan, W. Li, B. Balasubramanian, D. J. Sellmyer, and G. C. Hadjipanayis**

Single crystal $SmCo_5$ nanoparticles with an average size of 3.5 nm are produced by cluster-beam deposition. When deposited without matrix, the nanoparticles showed a super-paramagnetic behavior with a blocking temperature of 145 K. Dispersion of the $SmCo_5$ nanoparticles in a carbon matrix results in an increase in both the coercivity and the blocking temperature. Room temperature coercivities as high as 12 kOe are obtained for the first time in mono-layers of $SmCo_5$ nanoparticles dispersed in C matrix. δM plots show that the interactions in the samples are of exchange type, which can decrease the overall effective anisotropy and coercivity according to the random-anisotropy model. Coercivity is found to be inversely proportional to the packing density of the particles. $SmCo_5$ nanoparticles with high coercivity are potential candidates for the next generation ultra high-density magnetic recording media.

1. Introduction

Research to produce high-anisotropy magnetic nanoparticles with good magnetic properties without post-annealing has attracted much interest in recent years due to their potential use in high-density recording media and nano-composite magnets. From the scientific point of view, the effect of nano dimensions on the fundamental properties of the hard magnetic materials, (such as FePt and Sm-Co), has also attracted much interest from the scientific community.[1–3] The next generation ultra-high-density magnetic recording media require even smaller hard magnetic nanoparticles. However, the super-paramagnetic limit stands as an obstacle.[4] One way to overcome this problem is to use particles with higher magnetocrystalline anisotropy. Two such alloys are $SmCo_5$ and FePt whose high anisotropy values lead to the superparamagnetic sizes of 2.2 and 2.8 nm, respectively.[1,5] The need for a heat treatment to obtain the high anisotropy fct (L_{10}) phase[6] makes the latter alloys unattractive. Although some successful work has been done for the one-step fabrication of the FCT FePt nanoparticles, the properties are specific to the preparation techniques used.[14,17] On the other hand, rare earth based alloys are highly reactive to oxidation and require a thick protective layer while FePt has excellent corrosion resistance which makes it a good candidate for a longer term stability of the end product.[7]

Recent studies for the preparation of magnetically hard nanoparticles have been focused on three techniques; ball milling,[8–10] chemical synthesis[11–13] and cluster beam deposition (CBD).[14–22] The latter technique is the most prominent of all due to the high purity of the final product and the adaptability of the technique to current recording industry production lines.[23,24]

Recently, YCo_5 nanoparticles with good magnetic properties have been produced via the CBD teqhnique.[19] Our group's early attempt's to produce Sm-Co nanoparticles with high anisotropy using the CBD technique[21] have failed due to the technical problems with the construction of the gun and the oxidation problem. Since then considerable amount of upgrade has been done on the system. The biggest problem was the oxidation in the case of rare earth based alloys. This has been mostly resolved by using a research quality Grade 6 Argon with inclusions of 0.5 ppm of oxygen and 1 ppm of water, which with the addition of oxygen scavengers goes down to ppb. In addition, the aggregation chamber has been moved outside of the main chamber and modified according to the gas flow simulations for a better control of the particle crystallanity and size[26,27]. Even though there have been some studies on Sm-Co nanoparticles produced by the cluster beam deposition,[18–22] the expected high coercivity values have not yet been achieved. We strongly believe that the reason for the lower coercivities obtained in the $SmCo_5$ nanoparticles is the strong exchange interactions among the particles. For non-interacting single domain nanoparticles,[25] the reversal mechanism is dominated by coherent rotation. Any interactions present in the system will alter the reversal mechanism to incoherent magnetization rotation with lower coercivity.

In order to prove the above hypothesis, we have prepared different sets of samples where we varied the separation of $SmCo_5$ nanoparticles by dispersing them in a C matrix and investigated the effect of inter-particle interactions on the magnetic properties of the system.

Dr. O. Akdogan, Dr. W. Li, Prof. G. C. Hadjipanayis
Department of Physics and Astronomy
University of Delaware
Newark, DE 19716, USA
E-mail: hadji@udel.edu
Prof. D. J. Sellmyer, Dr. B. Balasubramanian
Department of Physics and Astronomy and Nebraska Center for Materials and Nanoscience
University of Nebraska
Lincoln, NE 68588, USA

DOI: 10.1002/adfm.201201353

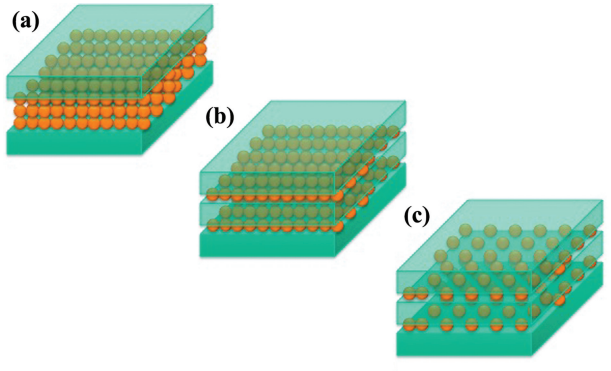

Figure 1. Schematic illustration of the distribution of the nanoparticles in the granular films, a) granular film without matrix, b) vertical separation by C layers, c) inter-layer separation in addition to vertical separation by C layers.

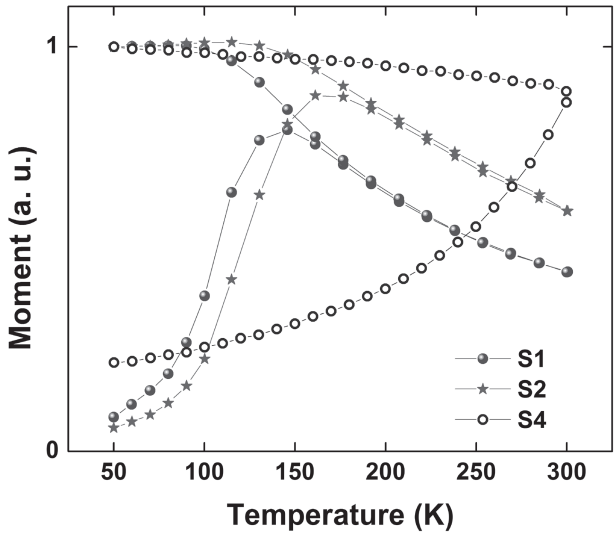

Figure 3. ZFC and FC curves at 150 Oe for sample S1, S2, and S4.

2. Results and Discussions

Three types of granular film have been deposited as illustrated schematically in **Figure 1**. A granular film of $SmCo_5$ nanoparticles without the matrix (labeled as sample S1) was prepared by depositing sequentially a 78 nm thick bottom C layer, a 168 nm $SmCo_5$ nanoparticles, and a 78 nm thick top C layer (Figure 1a). Dispersion of $SmCo_5$ nanoparticles in C were obtained by sequential depositions of 50 layers of $SmCo_5$ nanoparticles and C layers. Granular films with different $SmCo_5$ nanoparticle concentration were prepared by keeping the deposition time for $SmCo_5$ nanoparticles constant (10 s), while varying the thickness for the C layer (vertical separation, Figure 1b) to 6.5 nm (sample S2), 13 nm (sample S3), 26 nm (sample S4) and 52 nm (sample S5). In addition, a separate sample with $SmCo_5$ deposition time 5 s and C layer thickness 13 nm (sample S6) was also prepared to observe the effect of interlayer separation (Figure 1c).

We have successfully produced[18] single crystal $SmCo_5$ (previously called incorrectly $SmCo_7$ due to slight off stoichiometry of the as prepared 1:5 particles; however, recent SAED and EDS data show the 1:5 structure and composition, respectively) nanoparticles with an average size of 3.5 nm (**Figure 2**a). Selected area electron diffraction (SAED) pattern is indexed to the 1:5 structure and the fringe spacing of 2.1 Å corresponds to the (111) planes of $SmCo_5$ (Figure 2a insets). Even though the particles were larger than the superparamagnetic size for bulk $SmCo_5$ (2.2 nm), superparamagnetic behavior has been observed for sample S1 with a blocking temperature T_B of 145 K as shown in the zero-field cooled (ZFC) and field-cooled (FC) magnetization curves (**Figure 3**). Anisotropy constant K can be estimated roughly from T_B following the relation for single-domain particles;[5]

$$K = \frac{25kT}{V} \quad (1)$$

where k, T, K and V are the Boltzmann constant, temperature, anisotropy constant and the particle volume, respectively. For the sample with the particle size of 3.5 nm and using the blocking temperature of 145 K, the calculated K value from the above equation is 2.2×10^7 erg/cc. This value is considerably lower from the bulk value for this alloy, which is 1×10^8 erg/cc. There have been several explanations for this unusual behavior, including surface defects due to the high surface to volume ratio,[28] composition deviation in the particles and lack of crystallinity. However, the energy associated with CBD technique is much smaller compared to ball milling to create defects; EDS analysis showed a fairly uniform composition throughout the sample and HRTEM shows (Figure 2a inset) that the particles are fully crystalline. As we mentioned above, we believe that this may be the result of strong exchange interactions that lower the effective anisotropy and the coercivity of the 1:5 particles according to the random anisotropy model.[29]

Instead of sandwiching a large amount of the $SmCo_5$ nanoparticles between two single C layers (Figure 1a), the SmCo5 nanoparticle layer thickness was kept constant (deposition time 10 s) and the C layer thickness was varied from 6.5 to 52 nm (as previously

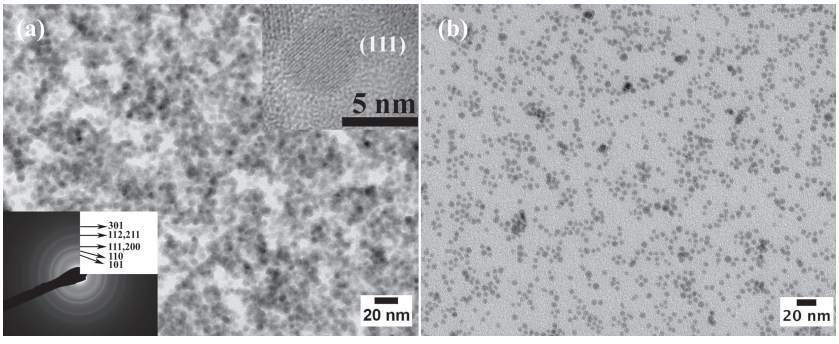

Figure 2. a) BF planar TEM image of $SmCo_5$ nanoparticles deposited for 10 s insets: HRTEM and SAED images and b) BF planar TEM image of $SmCo_5$ nanoparticles deposited for 5 s.

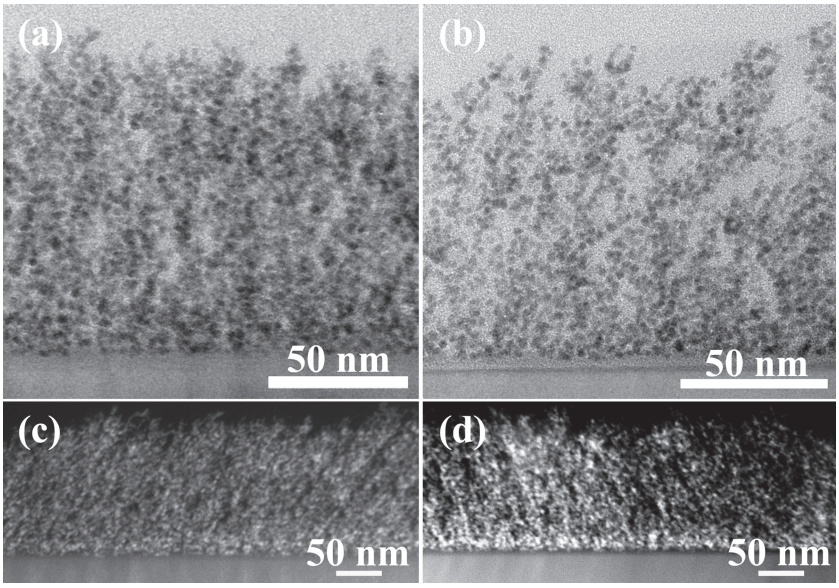

Figure 4. BF cross-sectioned images of a) S3, b) S4, c) corresponding HAADF-STEM image of samples S3 and d) S4.

shown in Figure 1b) to create a 50-layer stack. As a result we were able to separate the nanoparticles from each other. In order to observe the separation, TEM specimens from cross-sectioned samples have been prepared by ion milling. Bright field (BF) images of samples S3 and S4 show clearly that the particle size remained the same but the inter particle separation increased vertically (**Figure 4**a,b). Although the resultant morphology does not resemble the schematic representation in Figure 1b where sharp interfaces are present, this kind of morphology is expected. In the CBD process particle deposition into a matrix can be depicted as throwing steel balls on a pile of cotton. As expected, instead of just staying on top of the cotton pile, steel balls will go in to the cotton pile until their kinetic energy is zero. Same applies to the nanoparticles in the CBD technique. When highly energetic nanoparticles hit the Carbon, after the impingement, they will wander through the carbon until their energy becomes zero thus resulting in an arrangement of SmCo nanoparticles dispersed in C matrix. Furthermore, thicker carbon will stop the nanoparticles sooner thus the dispersion will be increased. High angle annular dark field scanning transmission electron microscopy (HAADF-STEM) image of S3 and S4 further demonstrates the separation of nanoparticles (Figure 4c,d). Besides the interactions present in the vertical direction, there are also interactions between nanoparticles in each layer of the stack. In order to show the effects of interlayer interactions, the $SmCo_5$ nanoparticle deposition time was reduced to 5 s while the C layer was kept at 13 nm, sample S6 (Figure 2b). Compared to 10 s $SmCo_5$ deposition time (Figure 2a) particles are farther apart. Consequently, the interlayer separation increased.

As compared to the granular film deposited without matrix S1, $SmCo_5$ nanoparticles dispersed in C are ferromagnetic at 300 K as shown in **Figure 5**. Interestingly, the coercivity (H_c) increases from 0.7 to 12 kOe in these samples by varying the thickness of the C layer from 6.5 to 52 nm as shown in **Figure 6**; this is presumably due to the increase of the inter-particle separation. Concentration of the $SmCo_5$ nanoparticles in the Carbon matrix is estimated from EDS (Figure 6). As the concentration decreases (separation increases) the coercivity of the granular films increases. Furthermore, the coercivity of sample S6 (inter-layer separated) is found to be 8.6 kOe as compared to the value of 5.5 kOe found in sample S3 (same C thickness). This result further suggests that an increase in the inter-particle separation causes a coercivity increase.

In addition to this, ZFC and FC magnetization curves of the S4 showed (Figure 3) that the blocking temperature of the sample is above RT, which in turn is an indication of an increase of the effective anisotropy of the system (Equation 1).

This rapid decrease of coercivity and effective anisotropy with a reduction in inter-particle separation can be explained by the random anisotropy model. According to this model, the anisotropy of an assembly of nanoparticles is decreased substantially due to the exchange interactions present in the system. The overall

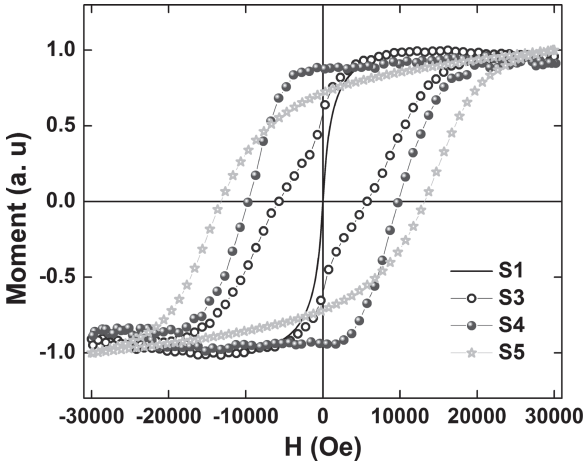

Figure 5. Room temperature hysteresis loops of $SmCo_5$ nanoparticles dispersed in C matrix.

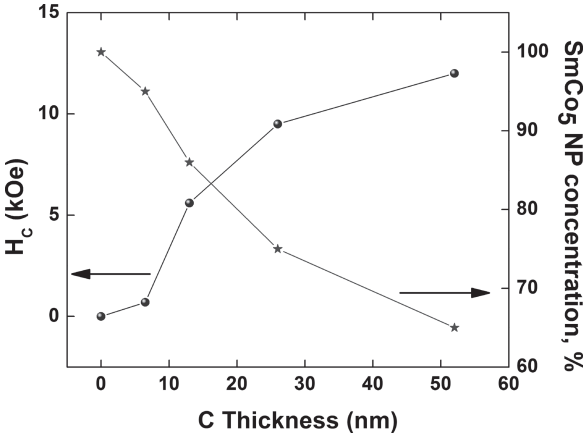

Figure 6. Coercivity and the concentration of $SmCo_5$ nanoparticles (NP) as a function of C thickness.

anisotropy of the system for the case of exchange length bigger than the particle size can be written as follows;[29,30]

$$\langle K \rangle = K_1 \left(\frac{D}{L_{ex}^{ef}} \right)^{3/2} \quad (2)$$

where K_1, D and L^{ef}_{ex} are anisotropy constant, particle size and the effective exchange length, respectively. This new effective exchange length can be defined as $L_{ex}^{ef} = \sqrt{A/\langle K \rangle}$ which is obtained by substituting for K_1 the mean anisotropy in the equation for the exchange length ($L_{ex} = \sqrt{A/K_1}$). Stronger interactions, due to the higher concentration of $SmCo_5$ nanoparticles, increase L^{ef}_{ex} and as a result the magneto-crystalline anisotropy is suppressed considerably.

Consequently, the coercivity of the system is reduced following the relation:[28,29]

$$H_C = p \frac{K_1^4 \times D^6}{J_S \times A^3} \quad (3)$$

where p, K_1, D, J_S and A are a material parameter, anisotropy constant, particle size, saturation magnetic polarization and exchange stiffness, respectively. It is noteworthy to mention here that the particle size is same for all samples. The most significant feature of the above analysis is the strong variation of H_C with the fourth power of the anisotropy constant K^4_1. Therefore, even a small reduction in the overall anisotropy of the system results in a considerable drop of effective coercivity.

Although A is a characteristic constant for each ferromagnetic (FM) material related to atomic exchange interactions that depends on the crystal structure, one should also consider the so called average or effective stiffness constant (A_{ef}) in the case of interparticle exchange interactions which depends on the microstructure of a system.[29–32] Previous reports on micromagnetic simulations in recording media with induced exchange stiffness showed a clear drop in anisotropy by increasing the value of A_{ef}.[33,34] Direct calculation or prediction of A_{ef} could be quite complicated for multi-phase systems where both phases are FM. This won't be a simple volume average but rather determined by the inverse averaging of the local exchange constants.[32] However, for the granular films examined in this study the second phase is NM and the size doesn't change thus the A_{ef} is directly proportional to the concentration (v) of the hard phase in the granular films ($A_{ef} \propto v$). In other words, a higher concentration of the hard phase will increase the inter-particle exchange interactions thus increase the A_{ef} (larger L^{ef}_{ex}) and consequently reduce the effective anisotropy of the system which is directly and effectively measured by H_C (Equation 3) and T_B (Equation 1).

To determine the type of particle interactions present in the samples, we studied the remenance curves. Isothermal Remanent Demagnetization (IRM) curves have been obtained on thermally demagnetized samples. Positive fields from 0 to 3 T were applied and then were removed and the remanence magnetization was measured. Direct Current Demagnetization (DCD) curves on the other hand, were obtained by applying magnetic field of 3 Tesla followed by a negative field (from 0 to −3T) which was then removed to measure the remennant magnetization (**Figure 7**). For a group of non-interacting particles with uniaxial anisotropy these two remanence values follow the relation:[35–37]

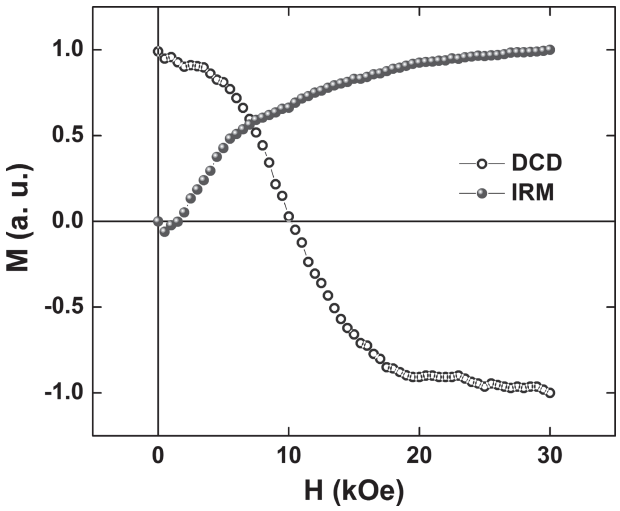

Figure 7. IRM and DCD curves of sample S3.

$$M_{DCD}(H) = 1 - 2M_{IRM}(H) \quad (4)$$

Equation 4 can be modified as follows:

$$\delta M(H) = M_{DCD}(H) - \left(1 - 2M_{IRM}(H)\right) \quad (5)$$

δM equal to 0 represents the case with no interactions present. Any deviation from zero is attributed to the presence of interactions in the system, which could be either dipolar for negative δM values or exchange for positive δM values. **Figure 8** shows the δM plots for samples S2, S3, S4, and S5. δM plots prove the existence of exchange interactions. The interactions decrease by increasing the C deposition time, which almost diminishes in the positive side for sample S5. As mentioned before, the particle size stayed the same for all samples.

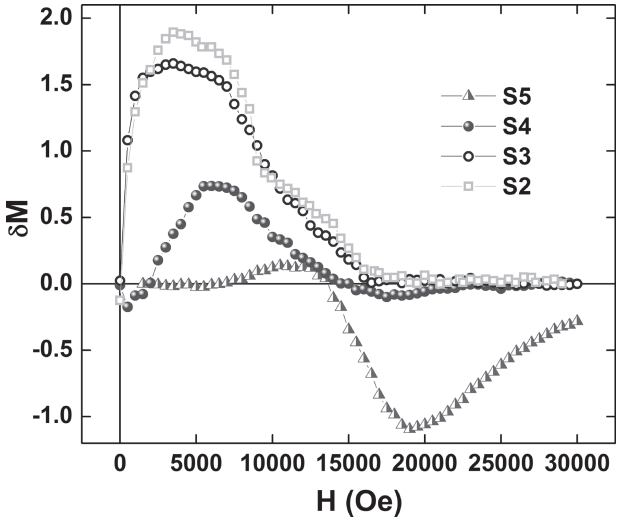

Figure 8. δM curves of samples S2, S3, S4, and S5.

Accordingly, the overall anisotropy (Equation 2) becomes only inversely proportional to the exchange length ($L^{ef}_{ex}{}^{-3/2}$), which varies with the exchange interaction. The decrease of exchange interaction by separation (lower $SmCo_5$ nanoparticle concentration Figure 6) causes a reduction in the L^{ef}_{ex} size, which in turn reflects itself as an increase in the overall anisotropy. Consequently, the observed coercivity increase with the decrease of exchange interaction is consistent with the prediction of random anisotropy model (Equation 3). Exchange length can be estimated for the case of sample without matrix by using the value of K estimated from the blocking temperature (145 K). Equation 2 predicts 10.2 nm for L^{ef}_{ex} which is almost three times the actual particle size of 3.5 nm.

According to the Stoner–Wolfhart model for a group of non-interacting randomly oriented nanoparticles with uniaxial anisotropy the reduced remanence (M_R/M_S) should be 0.5. Therefore, in addition to the coercivity decrease, interactions in the system can be observed via the increase of the reduced remanence. Reduced remanence indeed decreases from 0.96 for the S4 to 0.726 for the S5, thus shows the reduction in the exchange interaction. The remanence in sample S3 is lower because of the constricted loop due to inhomogeneous packing.

It is important to point out that the previous reports on the C addition showed considerable coercivity improvement in the Sm-Co alloys. However, it has been realized that that the coercivity improvement is due to the grain refinement in low C regime and grain boundary phase formation (Sm_2C_3) in high C regime which insulates the grains from each other.[38] Furthermore, ternary phase studies of the Sm-Co-C showed that C is not soluble in $SmCo_5$ even at 900 °C.[39] Consequently, in our samples C just acts as a separator between the particles to reduce the exchange interactions.

The first derivative of the DCD curve corresponds to the irreversible dc susceptibility, χ_{irr} which represents the switching field distribution in the system.[35–37] Narrow switching field distribution (SFD) is needed for ultra high density magnetic recording media in order to switch the bits completely with a given applied field. χ_{irr} curve for the sample S4 can be seen from **Figure 9**. The observed SFD is much narrower than other reports[40] even for non-aligned samples showing a peak at around 10 kOe.

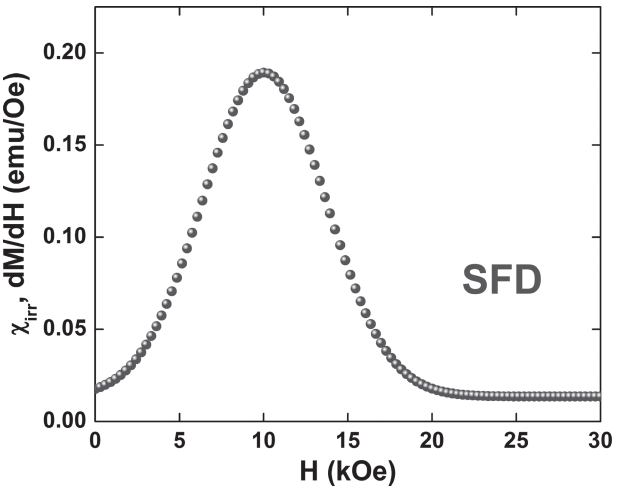

Figure 9. Switching field distribution for sample S4.

3. Conclusions

$SmCo_5$ nanoparticles have been successfully produced and dispersed in a carbon matrix with the cluster beam deposition technique. Poor dispersion of the nanoparticles resulted in a moderate room temperature coercivity, which is attributed to a considerable anisotropy decrease according to the random anisotropy model. Room temperature coercivities of as much as 12 kOe have been achieved by embedding the particles in a C matrix (for 52 nm C layer) where the inter-particle distance has been increased substantially resulting in a significant decrease of exchange interactions. A further improvement in the magnetic properties is possible by increasing the C layer thickness, however $SmCo_5$ target thickness limits the prolonged deposition times. Switching field distribution for the as-made nanoparticles is narrow which makes them a good candidate for the next generation ultra high-density recording media. Results of this work can be generalized to other closely packed particle systems wherever low coercivity cannot be explained otherwise. Cluster beam deposition could be the key technique to produce high coercivity RE-TM nanoparticles without post annealing.

4. Experimental Section

Schematic illustration and detailed description of the cluster-beam deposition system can be found elsewhere.[13,17] The base pressure in the sputtering chamber was 2×10^{-7} Torr and high purity Ar (99.9999%) was used for the deposition with a pressure of 5 mTorr inside the main chamber and 1 Torr inside the Cluster Gun (CG). A DC power of 25 and 24 W was applied to the $SmCo_5$ (sputtering rate ~3.6 Å/s) and C (sputtering rate = 2.6 Å/s) targets, respectively. Carbon thickness has been varied between 6 to 52 nm. Samples were sputtered on 500-µm-thick Si (100) wafers. Microstructure characterization and composition analyses of the samples were performed with JEOL JEM-3010 and JEM-2010F Transmission Electron Microscopes (TEM) and JSM 6330F Scanning Electron Microscope (SEM). Magnetic measurements at room temperature and below were made with a Quantum Design Versalab vibrating sample magnetometer with a maximum field of 3 T.

Acknowledgements

The authors thank Dr. A. M. Gabay for helpful discussions. Work supported by DOE DE-FG02-04ER4612 at Delaware and DOE DE-FG02-04ER46152 at Nebraska.

Received: May 18, 2012
Revised: November 21, 2012
Published online: February 6, 2013

[1] O. Gutfleisch, M. A. Willard, E. Bruck, C. H. Chen, S. G. Sankar, J. P. Liu, *Adv. Mater.* **2011**, *23*, 821.
[2] M. E. McHenry, D. E. Laughlin, *Acta Mater.* **2000**, *48*, 223.

[3] G. C. Hadjipanayis, *J. Magn. Magn. Mater.* **1999**, *200*, 373.
[4] N. A. Frey, S. Sun, *Magnetic Nanoparticle for Information Storage Applications. Inorganic Materials*, CRC Press, Boca Raton, Florida **2010**, pp. 33–68.
[5] B. D. Cullity, *Introduction to Magnetic Materials*. Addison-Wesley, Reading, MA **1972**.
[6] L. Colak, G. C. Hadjipanayis, *IEEE Trans. Magn.* **2009**, *45*, 4081.
[7] O. Gutfleisch, J. Lyubina, K. H. Müller, L. Schultz, *Adv. Eng. Mater.* **2005**, *7*, 208.
[8] E. M. Kirkpatrick, S. A. Majetich, M. E. McHenry, *IEEE Trans. Magn.* **1996**, *32*, 4502.
[9] N. G. Akdogan, G. C. Hadjipanayis, D. J. Sellmyer, *J. Appl. Phys.* **2009**, *105*, 07A710.
[10] N. G. Akdogan, G. C. Hadjipanayis, D. J. Sellmyer, *Nanotechnology* **2010**, *21*, 295705.
[11] H. Gu, B. Xu, J. Rao, R. K. Zheng, X. X. Zhang, K. K. Fung, C. Y. C. Wong, *J. Appl. Phys.* **2003**, *93*, 7589.
[12] T. Matsushita, T. Iwamoto, M. Inokuchi, N. Toshima, *Nanotechnology* **2010**, *21*, 095603.
[13] Y. Hou, Z. Xu, S. Peng, C. Rong, J. P. Liu, S. Sun, *Adv. Mater.* **2007**, *19*, 3349.
[14] O. Akdogan, W. Li, G. C. Hadjipanayis, R. Skomski, D. J. Sellmyer, *J. Appl. Phys.* **2012**, *111*, 07B535.
[15] J. M. Qiu, J. P. Wang, *Appl. Phys. Lett.* **2006**, *88*, 192505.
[16] J. M. Qiu, J. Bai, J. P. Wang, *Appl. Phys. Lett.* **2006**, *89*, 222506.
[17] X. Liu, S. He, J. M. Qiu, J. P. Wang, *Appl. Phys. Lett.* **2011**, *98*, 222507.
[18] O. Akdogan, W. Li, G. C. Hadjipanayis, D. J. Sellmyer, *J. Nanopart. Res.* **2011**, *13*, 7005.
[19] B. Balasubramanian, R. Skomski, X. Z. Li, S. R. Valloppilly, J. E. Shield, G. C. Hadjipanayis, D. J. Sellmyer, *Nano. Lett.* **2011**, *11*, 1747.
[20] B. Balasubramanian, R. Skomski, X. Z. Li, V. R. Shah, S. R. Valloppilly, G. C. Hadjipanayis, J. E. Shield, D. J. Sellmyer, *J. Appl. Phys.* **2011**, *109*, 07A707.
[21] S. Stoyanov, V. Skumryev, Y. Zhang, Y. Huang, G. C. Hadjipanayis, J. Nogués, *J. Appl. Phys.* **2003**, *93*, 7592.
[22] J. Tuaillon-Combes, M. Négrier, B. Barbara, W. Wernsdorfer, M. Treilleux, P. Mélinon, O. Boisron, A. Perez, *Int. J. Nanosci.* **2003**, *2*, 75.
[23] C. Binns, K. N. Trohidou, J. Bansmann, S. H. Baker, J. A. Blackman, J. P. Bucher, D. Kechrakos, A. Kleibert, S. Louch, K. H. Meiwes-Broer, G. M. Pastor, A. Perez, Y. Xie, *J. Phys. D Appl. Phys.* **2005**, *38*, R357.
[24] K. Wegner, P. Piseri, H. V. Tafreshi, P. Milani, *J. Phys. D: Appl. Phys.* **2006**, *39*, R439.
[25] E. C. F. R. S. Stoner, E. P. Wohlfarht, *Phil. Trans. R. Soc. A* **1948**, *240*, 599.
[26] P. Liu, Ph.D. Thesis, University of Delaware, USA **2009**.
[27] O. Akdogan, Ph.D. Thesis, University of Delaware, USA **2012**.
[28] A. Giri, K. Chowdary, S. A. Majetich, *Mater. Res. Soc. Symp. Proc.* **1999**, *577*, 197.
[29] G. Herzer, *IEEE Trans. Magn.* **1990**, *26*, 1397.
[30] G. Herzer, *Scripta Metall. Mater.* **1995**, *33*, 1741
[31] G. Herzer, *Properties and Applications of Nanocrystalline Alloys from Amorphous Precursors* (Eds: B. Idzikowski, P. Svec, M. Miglierini), Kluwer Academic Publishers, Netherlands **2005** pp. 15–34.
[32] G. Herzer, *IEEE Trans. Magn.* **1989**, *25*, 3327.
[33] E. Miyashita, R. Taguchi, N. Funabashi, T. Tamaki, H. Okuda, *IEEE Trans. Magn.* **2002**, *38*, 2075.
[34] E. Miyashita, K. Kawana, H. Shiino, N. Hayashi, *J. Magn. Magn. Mater.* **2008**, *320*, 2921.
[35] R. Alben, J. J. Becker, M. C. Chi, *J. Appl. Phys.* **1978**, *49*, 1653.
[36] R. W. Chantrell, K. O'Grady, *Appl. Magn.* **1994**, *253*, 113.
[37] K. O'Grady, R. W. Chantrell, *Proceedings of the International Workshop on Studies of Magnetic Properties of Fine Particles* **1992**, p. 93.
[38] S. Aich, J. E. Shield, *J. Alloys Compd.* **2006**, *425*, 416.
[39] H. H. Stadelmaier, N. C. Z. Liu, *Metallkunde* **1985**, *76*, 585.
[40] A. Sebt, M. Akhavan, *J. Magn. Magn. Mater.* **2001**, *237*, 111.